N87-26443

NEAR-OPTIMUM DESIGN OF THE InP HOMOJUNCTION SOLAR CELL

Chandra Goradia and James V. Geier
Cleveland State University
Cleveland, Ohio

Irving Weinberg
NASA Lewis Research Center
Cleveland, Ohio

Using a fairly comprehensive model, we have done a parametric variation study of the InP n+p homojunction solar cell for AMO, 25°C operation. The results of this study are presented. These results indicate that an efficiency of about 20.5% should be realistically possible in a shallow homojunction InP solar cell with near-optimum design.

INTRODUCTION

Results obtained so far indicate that InP solar cells show a much greater tolerance to 1MeV electron and 10MeV proton irradiation than Si and GaAs solar cells [1]. In addition, InP cells can be annealed at a relatively low temperature of about 100°C [2] and are even annealed under minority carrier injection under a forward bias [3]. For these reasons, InP cells show great promise for space applications and there is now considerable interest in developing these cells for high efficiency.

Currently, the best InP cells have exhibited a total area, AMO, 25°C efficiency of 16% [4]. This efficiency needs to be significantly improved in order for InP cells to meet the long-term kW/kg, kW/m^2 and $/kW goals for space cells. There is thus a need to theoretically assess the realistic improvements in efficiency that may be possible for InP cells. To this end, we undertook to answer the following two questions: 1) What is the maximum realistically achievable AMO, 25°C total area efficiency in InP cells? 2) What is the optimum or near-optimum design of the cell in terms of its geometrical and material parameters which will yield this maximum efficiency?

To help us answer the above questions, we have developed a fairly comprehensive one-dimensional computer simulation model for the InP solar cell. This model takes into account position- and wavelength-dependent optical generation in the emitter, base, space-charge and BSF/substrate regions, doping-dependent mobilities and lifetimes (HSR and radiative) in all these regions, and realistic front and back surface recombination velocities. In addition, the model calculates the wavelength-dependent reflection coefficient for a given AR coating material and thickness and the series resistance for a given rectangular or circular grid design.

CALCULATED RESULTS

Using this model, we have done a parametric variation study to determine the maximum realistically attainable efficiency and near-optimum design of the cell. As a first step, to gain confidence in our model, we tried to fit our calculated results to the measured results on two InP cells made at Rensselaer Polytechnic Institute. Using only the diffusion lengths in the emitter and base and the effective lifetime in the space charge region as fitting parameters, we got excellent match with the measured curves of not just the illuminated I-V but also the spectral response and the I_{SC}-V_{OC}. In addition, our model predicted the same behavior of the performance parameters as a function of base doping as observed by Yamamoto et al [5].

Table 1 shows the near-optimum design parameters and best performance for each of three combinations of emitter and base dopings. It is seen that the best performance is obtained for relatively low emitter and base dopings of 5E17 and 1E16 cm^{-3} respectively, yielding a realistically attainable efficiency of ~20.5%. Our predicted values of V_{OC} are low because we have used conservatively low lifetimes and diffusion lengths. With somewhat longer lifetimes, V_{OC}'s up to about 915mV are predicted, with correspondingly higher efficiencies reaching 21.4%. Note the rather decent values of short circuit current density and fill factor, indicating that series resistance is not a problem even for the rather thin emitter of only 400Å.

Figures 1 and 2 show the cell output parameters versus emitter width and emitter doping respectively. The values of all other parameters are as listed under the Series C column in Table 1. The vertical arrows in these and other figures indicate nominal values of the independent variable.

It is seen from Figure 1 that for the chosen grid design the cell efficiency monotonically decreases with increasing width of the emitter, indicating that the emitter should be as narrow as is realistically possible, around 400 to 600Å. The primary cause of efficiency reduction with increasing emitter width is the reduced collection of photogenerated carriers, as evidenced by a significant decrease in the short circuit current density. A secondary cause is the increased recombination with a large emitter volume, causing a reduction in V_{OC} with increasing emitter width.

Figure 2 shows that there is a broad peak in the curve of cell efficiency versus emitter doping, with best results for an emitter doping between 4E17 and 8E17 cm^{-3}. At the rather low emitter dopings, below 1E17 cm^{-3}, it is the V_{oc} and FF which are low; on the other hand, all parameters, J_{sc}, V_{oc} and FF, decrease with increasing doping above 1E18 cm^{-3}. Thus, a relatively low emitter doping of ~5E17 cm^{-3} is ideal.

Figure 3 shows the performance parameters versus front surface recombination velocity (SRV). It is very likely that the 1E4 cm/s value of front SRV which we have used in our calculations is perhaps too low and a more realistic value should have been 1E5 to 2E5 cm/s. If that be the case, then we see from this figure that the maximum efficiency would come down from 20.35% to ~19.7% or, for the case of longer lifetimes, from 21.4% to ~20.7%. Note that because of the rather large diffusion velocity D/L in the emitter ($\gtrsim$1E4 cm/s), cell performance is barely affected by front SRV values smaller than a few times 1E4 cm/s.

In Figures 4 and 5 we show cell performance parameters versus base width and base doping respectively. It is seen that, up to a base width of 4μm, the V_{oc} monotonically decreases because of increased volume recombination, since base diffusion length is greater than 4μm, while I_{sc} increases with base width. The efficiency goes through a broad peak at a base width between 2.0 and 3.0μm. More interestingly, the V_{oc} increases and I_{sc} decreases with increasing base doping in such a manner that the efficiency decreases with increasing base doping. The ideal base doping seems to lie in the range 5E15 to 5E16 cm^{-3}. This is in conformation with the observed dependence of performance on base doping. In the present effort, our emphasis has been on optimum design only with respect to efficiency. We are in the process of incorporating into our model the fluence dependence of lifetime (in all regions of the cell) and of the front SRV and doing radiation damage simulation of the cell. It may then turn out that from the radiation tolerance point of view, base dopings around 5E16 cm^{-3} or somewhat higher may be desirable, as has been experimentally observed.

Figure 6 shows the components of light-generated current ($\approx I_{sc}$) from the various cell regions and Figure 7 shows the loss current components at open circuit, both as functions of the base doping. In Figure 6 it is seen that for base dopings less than 2E16 cm^{-3} nearly two-thirds of the light-generated current comes from the space charge region, slightly less than one-third from the emitter and only a very small amount from the base. This in spite of a very thin (400Å) emitter. This is because of the very high optical absorption coefficient of InP. This is very different from silicon solar cells where practically all of the light-generated current comes from the base, and also somewhat different from gallium arsenide solar cells where the base contributes significantly to the light-generated current. This difference may have a bearing on the improved radiation tolerance of InP solar cells compared to Si and GaAs solar cells. We are in the process of investigating this. On the other hand, as seen from Figure 7, the base is practically the sole contributor to the loss current at V_{OC}. This behavior is the same as in Si and GaAs solar cells. It is easily seen from Figures 6 and 7 why I_{SC} decreases and V_{OC} increases with increasing base doping.

CONCLUSIONS

Our theoretical modelling of the InP n^+ shallow homojunction solar cell allows us to draw the following inferences:

1. A maximum total area, 1AMO, 25°C efficiency slightly above 20% appears realistically possible.

2. A near optimum design of the cell would have emitter and base high quality layers (preferably, epitaxial) of thicknesses ~400Å and 2μm respectively and dopings 5E17 cm^{-3} and 1E16 respectively, with a good quality BSF/substrate layer of doping 2E18 to 5E18 cm^{-3}.

3. The light-generated current (~I_{SC}) is controlled primarily by the space charge and emitter regions while the open circuit voltage V_{OC} is controlled primarily by the properties of the base region.

REFERENCES

1. Yamaguchi, M.; Uemura, C.; and Yamamoto, A., "Radiation Damage in InP Single Crystals and Solar Cells," J. Appl. Phys. 55, 1429 (1984).

2. Yamaguchi, M.; Itoh, Y.; and Ando, K., "Room-Temperature Annealing of Radiation-Induced Defects in InP Solar Cells," Appl. Phys. Lett. 45, 1206 (1984).

3. Yamaguchi, M.; Ando, K.; Yamamoto, A.; and Uemura, C., "Minority-Carrier Injection Annealing of Electron Irradiation-Induced Defects in InP Solar Cells," Appl. Phys. Lett. 44, 432 (1984).

4. Yamaguchi, M.; Yamamoto, A.; Itoh, Y.; Uemura, C., "22% (AM 1.5, Active Area) Efficient and High Radiation Resistant InP Solar Cells," Proc. PVSEC II, Aug. 19-22, 1986, Beijing, China, pp. 573-576.

5. Yamamoto, A.; Yamaguchi, M.; and Uemura, C., "Fabrication of High-Efficiency n^+p Junction InP Solar Cells by Using Group VIb Element Diffusion into p-Type InP," IEE Trans. Elect. Dev. 32, 2780 (1985).

TABLE 1

Parameter	Series B	Series D	Series C
Performance:			
Short Ckt. Current Density J_{sc}, mA/cm^2	35.85	37.05	37.29
Open Ckt. Voltage V_{oc}, mV	875.1	877.4	877.7
Fill Factor FF, %	85.09	85.39	85.38
Conversion Efficiency η, %	19.44	20.22	20.35
General:			
Junction Area, cm^2	1.00	1.00	1.00
Total Illuminated Area, cm^2	0.94	0.94	0.94
Grid Coverage, %	6.00	6.00	6.00
SiO AR Coating, angstroms	750	750	750
Specific Contact Resistance, ohm-cm^2	1.0E-3	1.0E-3	1.0E-3
Intrinsic Carrier Concentration n_i, cm^{-3}	1.655E7	1.655E7	1.655E7
Calculated Series Resistance R_s, ohm	0.137	0.199	0.271
Front Surface Recombination Velocity S_F, cm/s	1.0E4	1.0E4	1.0E4
Space-Charge Region Dark Current Correction Factor	2.0E-2	2.0E-2	2.0E-2
n^+ Emitter:			
Width W_E, angstroms	400	400	400
Uniform Doping N_{dE}, cm^{-3}	5.0E18	1.0E18	5.0E17
Minority Carrier Mobility μ_{pE}, cm^2/Vs	40.0	75.0	100.0
Minority Carrier Lifetime τ_{pE}, ns	0.04	0.20	0.40
Minority Carrier Diffusion Length Length L_{pE}, μm	0.064	0.196	0.321
p Base:			
Width W_B, μm	2.00	2.00	2.00
Uniform Doping N_{aB}, cm^{-3}	5.0E16	5.0E16	1.0E16
Minority Carrier Mobility μ_{nB}, cm^2/Vs	3.55E3	3.55E3	4.25E3
Minority Carrier Lifetime τ_{nB}, ns	4.00	4.00	20.0
Minority Carrier Diffusion Length L_{nB}, μm	6.00	6.00	14.8
p^+ BSF/Substrate Layer:			
Width W_S, μm	250	250	250
Uniform Doping N_{aS}, cm^{-3}	5.0E18	5.0E18	5.0E18
Minority Carrier Mobility μ_{nS}, cm^2/Vs	2.46E3	2.46E3	2.46E3
Minority Carrier Lifetime τ_{nS}, ns	0.040	0.040	0.040
Minority Carrier Diffusion Length L_{nS}, μm	0.50	0.50	0.50
Effective SRV at BSF/Base Interface S_s, cm/s	1.26E4	1.26E4	2.51E3

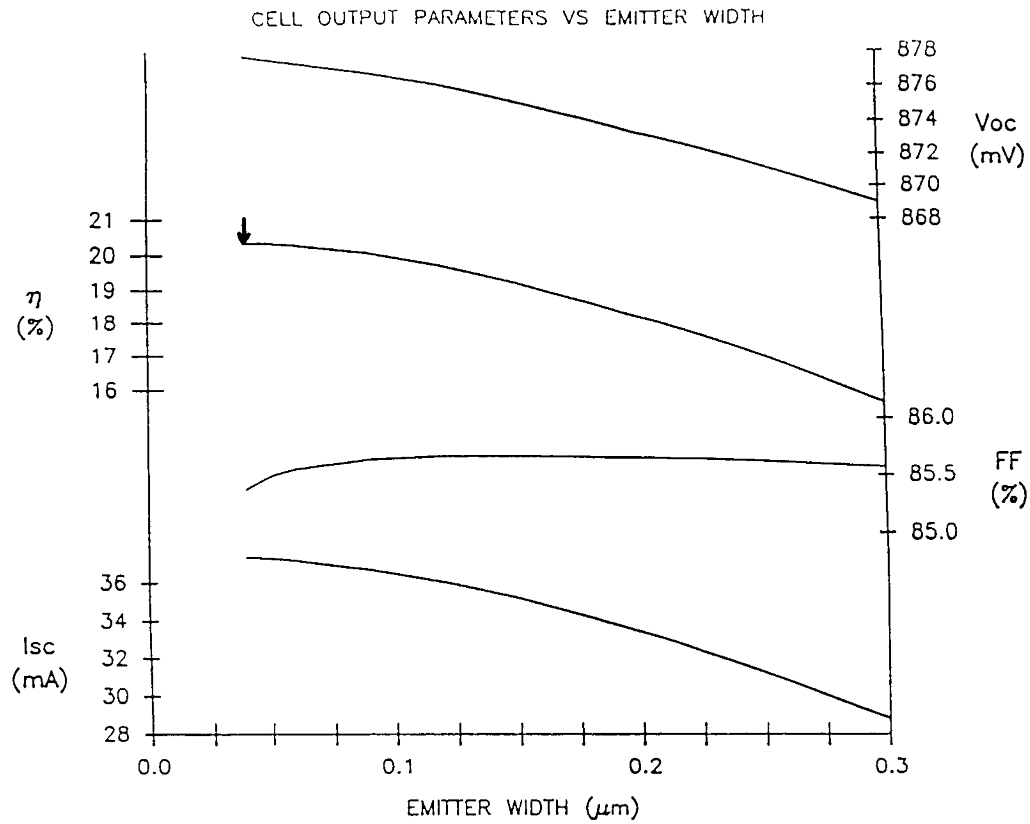

Figure 1

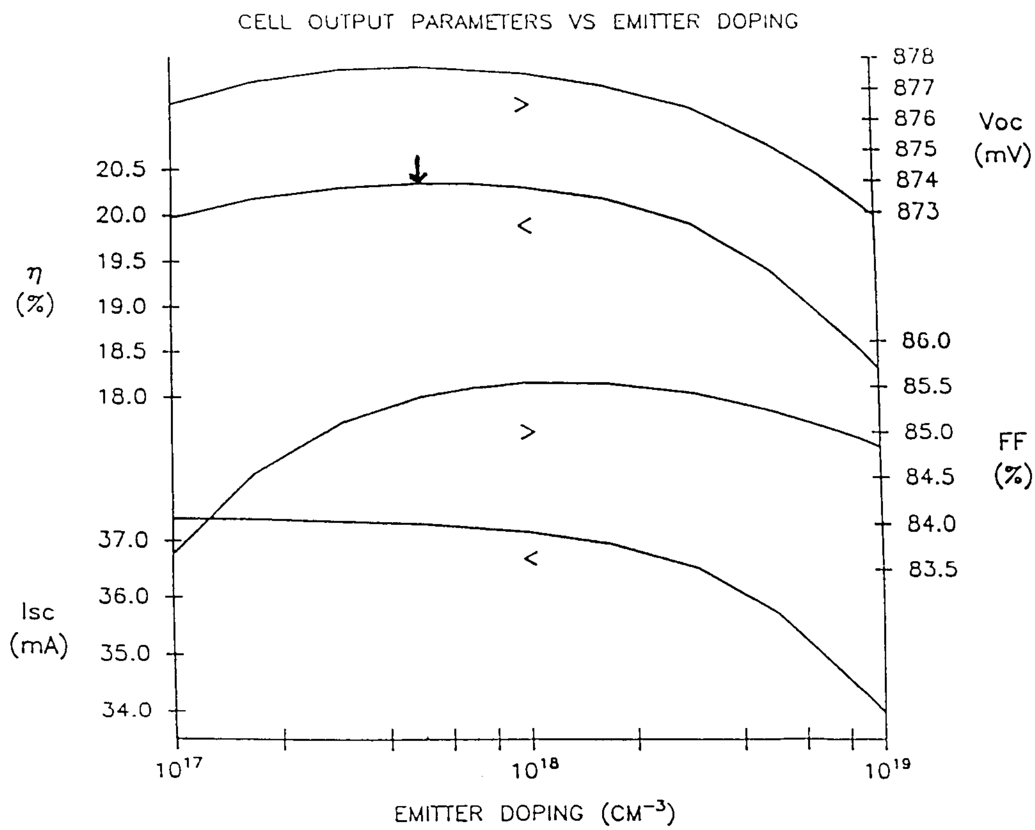

Figure 2

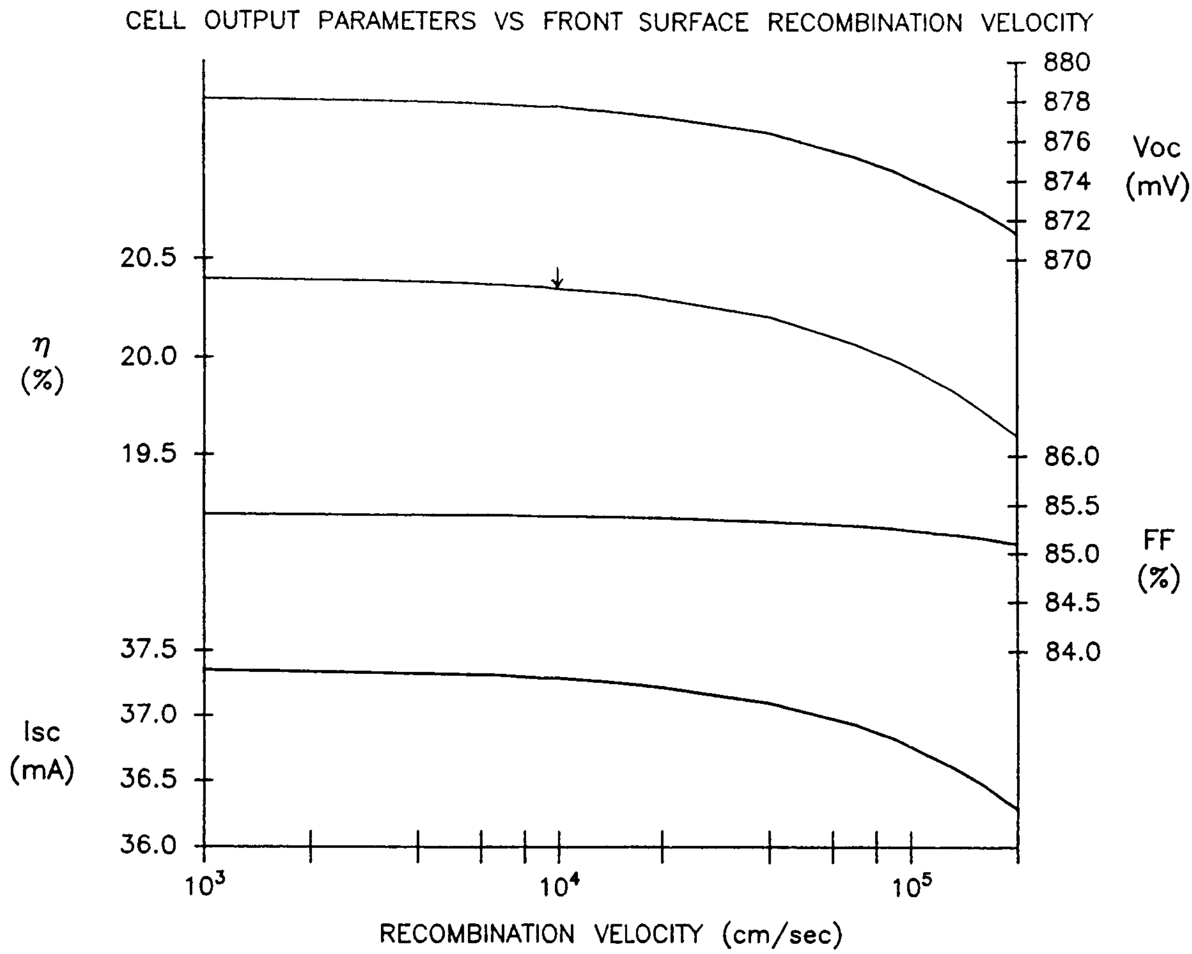

CELL OUTPUT PARAMETERS VS FRONT SURFACE RECOMBINATION VELOCITY
880
878
876
874
872
870
Voc
(mV)
20.5
20.0
19.5
η
(%)
86.0
85.5
85.0
84.5
84.0
FF
(%)
37.5
37.0
36.5
36.0
Isc
(mA)
10³
10⁴
10⁵
RECOMBINATION VELOCITY (cm/sec)

Figure 3

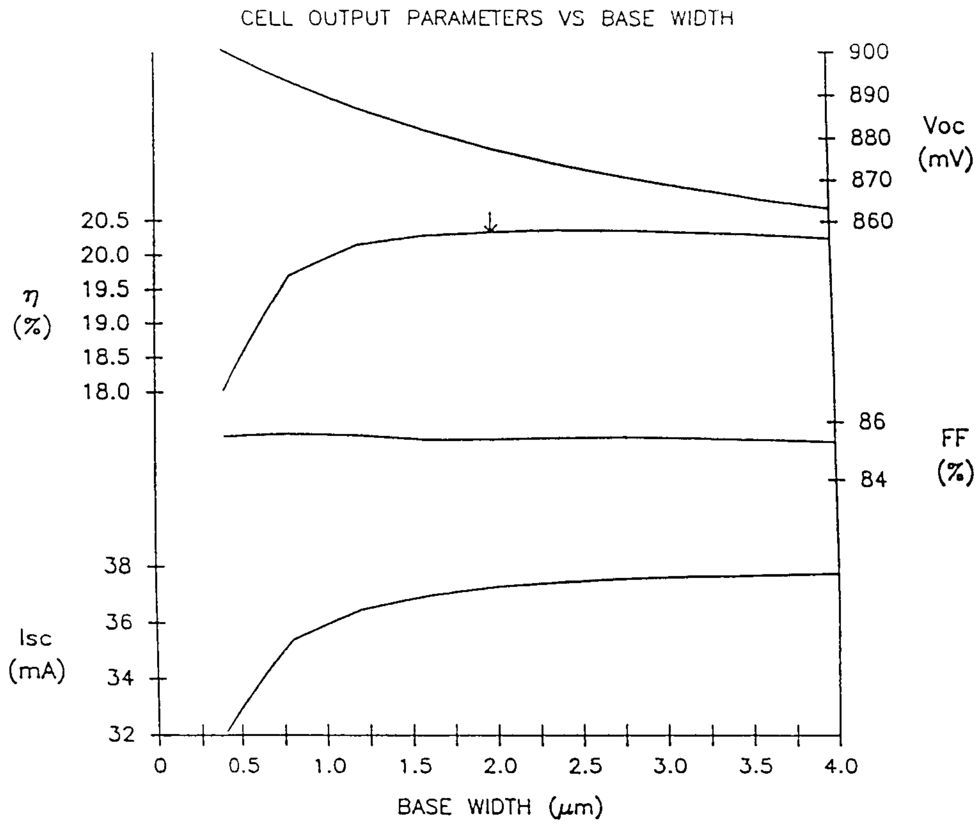

Figure 4

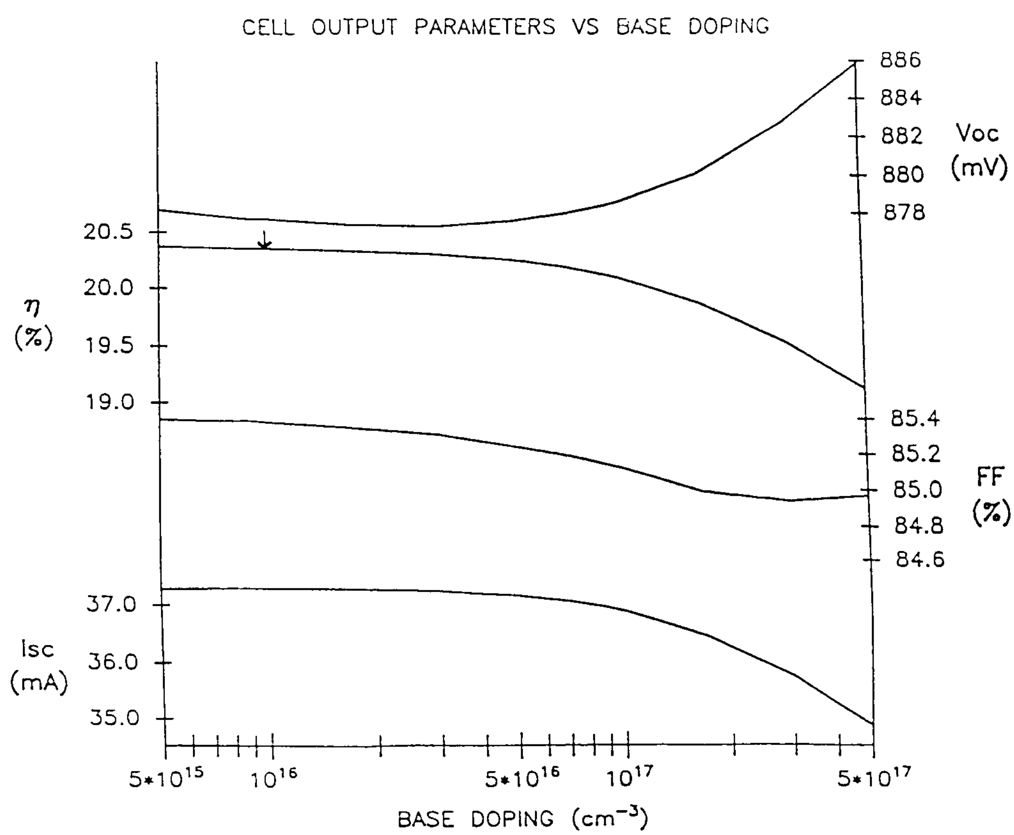

Figure 5

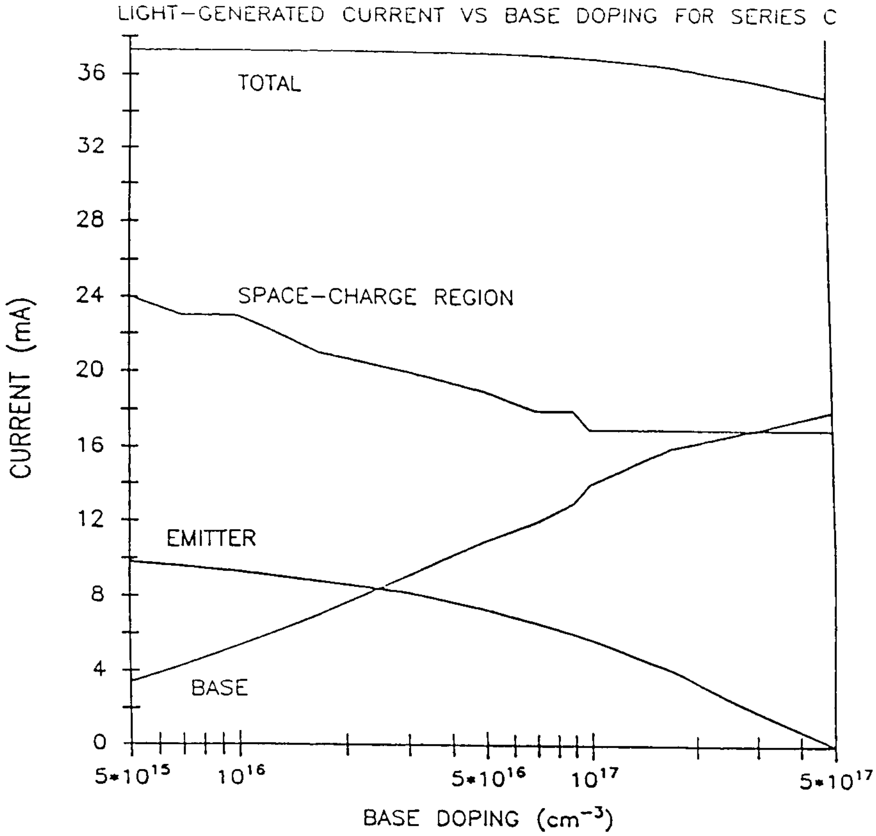

Figure 6

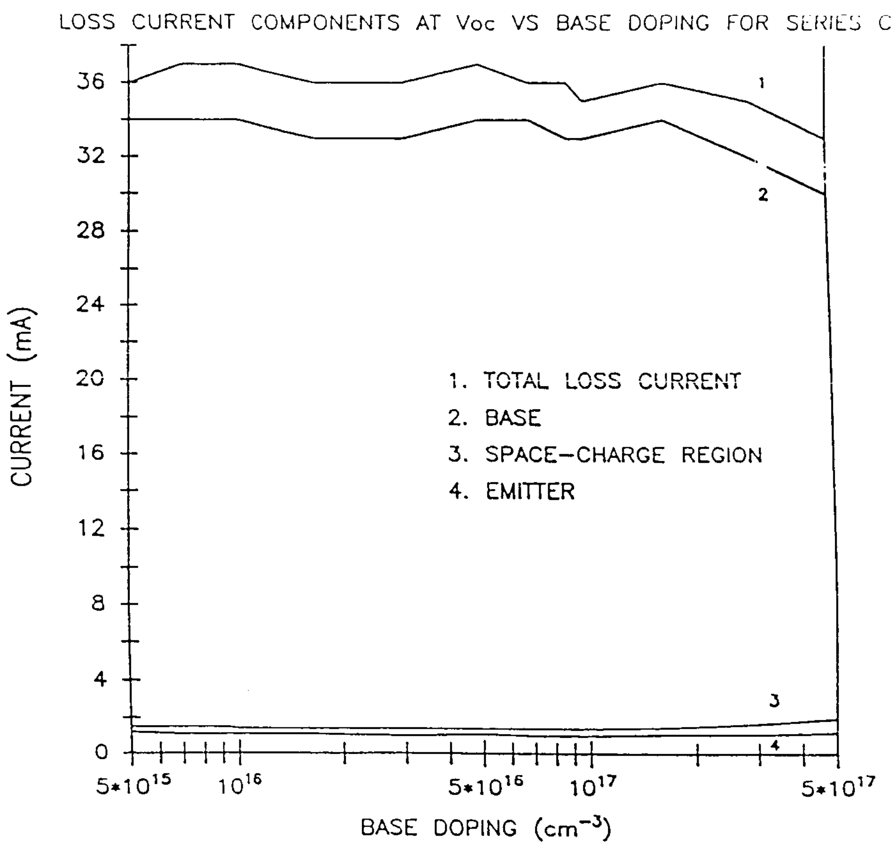

Figure 7